

**The OGLE Collection of Variable Stars:
Over 18 000 Rotating Variables toward the Galactic Bulge**

P. Iwanek¹, I. Soszyński¹, K. Stępień¹, S. Kozłowski¹, J. Skowron¹
A. Udalski¹, M. K. Szymański¹, M. Wrona^{4,1}, P. Pietrukowicz¹
R. Poleski¹, P. Mróz¹, K. Ulaczyk^{2,1}, D.M. Skowron¹,
M. Gromadzki¹, K. Rybicki^{3,1}, M.J. Mróz¹ and M. Ratajczak¹

¹ Astronomical Observatory, University of Warsaw, Al. Ujazdowskie 4,
00-478 Warsaw, Poland

² Department of Physics, University of Warwick, Gibbet Hill Road, Coventry,
CV4 7AL, UK

³ Department of Particle Physics and Astrophysics, Weizmann Institute of Science,
Rehovot 76100, Israel

⁴ Villanova University, Department of Astrophysics and Planetary Sciences,
800 Lancaster Ave., Villanova, PA 19085, USA

Received June 12, 2024

ABSTRACT

Stellar rotation, a key factor influencing stellar structure and evolution, also drives magnetic activity, which is manifested as spots or flares on stellar surface. Here, we present a collection of 18 443 rotating variables located toward the Galactic bulge, identified in the photometric database of the Optical Gravitational Lensing Experiment (OGLE) project. These stars exhibit distinct magnetic activity, including starspots and flares. With this collection, we provide long-term, time-series photometry in Cousins *I*- and Johnson *V*-band obtained by OGLE since 1997, and basic observational parameters, *i.e.*, equatorial coordinates, rotation periods, mean brightness, and brightness amplitudes in both bands. This is a unique dataset for studying stellar magnetic activity, including activity cycles.

Key words: *Stellar activity (1580), Starspots (1572), Stellar flares (1603), Flare stars (540)*

1. Introduction

Among the various phenomena observed in stars, rotation stands out as a fundamental aspect shaping their structure (Rivinius *et al.* 2013, Aerts *et al.* 2019) and evolution (Maeder and Meynet 2000). It is also responsible for the formation of magnetic fields through the dynamo mechanism (Parker 1955, Charbonneau 2013) and the inherently associated magnetic activity manifested in spots or flares (Irwin *et al.* 2009, Roettenbacher *et al.* 2016, Chowdhury *et al.* 2018, Iwanek *et al.* 2019).

Skumanich (1972) pioneered a groundbreaking study on stellar rotation and activity, laying the foundation for a new branch of astrophysics. One of the key findings of Skumanich's work revolves around the analysis of lithium abundance, indicating a decrease in its presence on stellar surfaces as stars age, particularly during the first dredge-up phase. Additionally, the author observed a decline in rotational velocity with increasing stellar age, attributed to magnetic braking, where the interaction of magnetic fields with stellar winds acts as a decelerating force. The final finding, based on CaII emission as an indicator of magnetic activity, revealed a diminishing trend between CaII emission (hence magnetic activity) and stellar age. The studies initiated by Skumanich (1972) are continued today under the name gyrochronology (Barnes 2007, Reinhold and Gizon 2015).

Measuring the rotation periods of stars is an important aspect of astrophysics. Active regions on stellar surfaces (spots) induce periodic or quasi-periodic brightness changes, enabling direct measurement of rotation periods (Irwin *et al.* 2009). This method ranks among the most commonly used techniques, albeit necessitating precise, long-term photometric observations, as variability caused by spots occurs with various periods (ranging from a fraction of a day to hundreds of days), with amplitudes typically smaller than 0.2–0.3 mag (Lanzafame *et al.* 2018, Iwanek *et al.* 2019, Distefano *et al.* 2023). Another widely used method for measuring rotation periods involves observing the CaII H and K emission lines (Baliunas *et al.* 1983, Gilliland and Fisher 1985, Salabert *et al.* 2016).

An intriguing phenomenon is the existence of stellar magnetic activity cycles. The first observations of the solar activity cycle were made by Schwabe (1844, 1845) by studying the migration of sunspots on the surface. Schwabe noticed that the sunspot migration pattern repeats approximately every 11 yr. Studying activity cycles is difficult because we do not directly observe spots on other stars. Additionally, such studies require long-lasting monitoring of the same stars to cover multiple activity cycles and measure their lengths with sufficient precision. Despite these difficulties, such studies are being successfully conducted (*e.g.*, Oláh *et al.* 2007, 2009, Mathur *et al.* 2014, Oláh *et al.* 2016, Montet *et al.* 2017, Reinhold *et al.* 2017, Martínez *et al.* 2022).

Contemporary large-scale sky surveys provide invaluable data in the context of the rotation and magnetic activity of hundreds of thousands of stars. Particular attention should be given to the data provided by the Gaia satellite with the Radial Velocity Spectrometer, based on which the stellar activity index has been determined for 2×10^6 stars in the Milky Way (Lanzafame *et al.* 2023). Reinhold *et al.* (2013), McQuillan *et al.* (2014) and Reinhold *et al.* (2023) measured the rotation periods for stars observed by the Kepler Space Telescope, while Davenport (2016) and Davenport *et al.* (2019) found flaring stars in the Kepler data. The flaring activity was also investigated using data from the Transiting Exoplanet Survey Satellite (TESS) mission by Crowley *et al.* (2024). Rotating stars have been discovered through ground-based surveys, such as the All Sky Automated Survey

(ASAS, Kiraga 2012, Kiraga and Stępień 2013), the All Sky Automated Survey for Supernovae (ASAS-SN, Jayasinghe *et al.* 2020), the Massive Compact Halo Objects (MACHO, Drake 2006) or the Optical Gravitational Lensing Experiment (OGLE, Iwanek *et al.* 2019).

In this study, we use data from the OGLE project, collected for nearly 30 yr, to find as many magnetically active stars as possible. Our main goal was to provide the astronomical community with long-term, two-band time-series photometry, which will undoubtedly be a treasure trove of knowledge about stellar magnetic activity. In the study by Iwanek *et al.* (2019), we utilized 12 660 objects published in this collection and analyzed in detail the relations between the observational properties of these stars, *i.e.*, rotation period, mean brightness, brightness amplitude, and color index. We also demonstrated the existence of two types of spots characterized by the dependence between changes in the color index and changes in the brightness. This collection includes the stars analyzed in the paper Iwanek *et al.* (2019) and nearly 6000 new objects classified as rotational variables.

This paper is organized as follows. In Section 2, we describe the OGLE project and its data. In Section 3 we outline the selection process of rotating variables, including measuring rotation periods methods. The mean brightness and brightness amplitude measuring methods are discussed in Section 4. In Section 5, we describe and discuss the entire collection of rotating variables, and we show many interesting objects with time-series photometry collected since 1997. Conclusions can be found in Section 6.

2. Observations and Data Reduction

The OGLE project can boast one of the longest-lasting large-sky survey conducting regular high-quality photometric observations in the history of astronomy. Historically, OGLE began its activities in 1992 (OGLE-I, Udalski *et al.* 1992) using the 1.0-m Swope Telescope located at the Las Campanas Observatory in Chile. Subsequently, with acquired funding, a dedicated telescope for the project, the 1.3-m Warsaw Telescope, was built at the Las Campanas Observatory, Chile, which in 1997 initiated the second phase of the project (OGLE-II, Udalski *et al.* 1997), thus beginning the regular monitoring of stars in the Galactic bulge (BLG) and the Magellanic Clouds. The project then went through two more phases: OGLE-III (2001-2009, Udalski 2003) and OGLE-IV (2010-today, Udalski *et al.* 2015), which mainly differed in field of view of the CCD camera used and in the larger monitored area of the sky, including the Galactic disk. The fourth phase of the project was interrupted for over two years in March 2020 due to the COVID-19 pandemic. The OGLE project resumed regular observations in August 2022.

The Warsaw Telescope is equipped with a mosaic CCD camera consisting of 32 chips, each with a resolution of $2k \times 4k$ px, resulting in approximately 268 million pixels. The field of view of the OGLE-IV camera is 1.4 square degrees with a pixel

scale of $0''.26$. As a part of the BLG survey, we regularly observe over 400 million stars located in an area of 182 square degrees. The OGLE-IV inner BLG footprint is presented in Fig. 1.

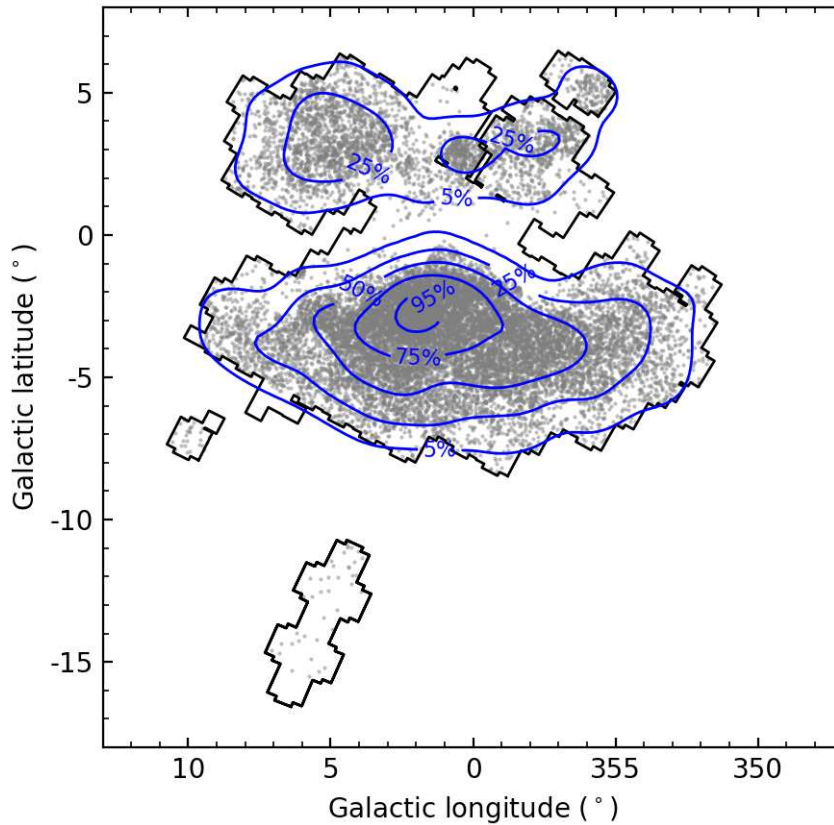


Fig. 1. Distribution of rotating stars in the sky toward the Galactic bulge. Gray points denote all rotating variables discovered in the OGLE-IV data, while black contours correspond to the OGLE footprint. With blue contours, we plot the normalized density of rotating variables with values: 95%, 75%, 50%, 25%, and 5%.

The OGLE observations are conducted in Johnson V (mean wavelength of $0.55 \mu\text{m}$) and Cousins I (mean wavelength of $0.81 \mu\text{m}$) filters. The vast majority of observations are taken in the I band, while V -band observations are much less frequent and generally performed to determine the $(V - I)$ color indices of the observed stars. The exposure times for the BLG fields are 100 s and 150 s for the I - and V -band, respectively.

A comprehensive overview of the instrumentation, photometric reductions, and astrometric calibrations for the OGLE-IV observations can be found in Udalski *et al.* (2015).

3. Selection and Classification of Rotating Variables

In large-scale sky surveys, rotating (spotted) variables are generally treated somewhat neglectfully, and searches devoted to these stars are rarely conducted. This is partly due to the difficulty of detecting them, as their quasi-periodic variability usually lacks a well-defined pattern, unlike, for example, pulsating or eclipsing stars. In the searches conducted as a part of this work, we began with a sample of 19 513 stars flagged as “spotted” during searches for other types of variable stars (*e.g.*, Soszyński *et al.* 2016, Udalski *et al.* 2018, Wrona *et al.* 2022). A common feature in the searches for any type of variable stars in the OGLE data is that the samples of stars are selected semi-automatically (using, *e.g.*, some cuts on periods, amplitudes, color indices, etc.) and then they are manually reviewed by experienced astronomers. For this reason, it was possible to identify stars exhibiting long-term modulation of amplitude and mean magnitude, which could potentially indicate the presence of spots on stellar surfaces. The presence of long-term brightness modulation over several to several dozen periods is directly related to magnetic activity and the presence of activity cycles. Such variability can be confused, for example, with semi-regular variations caused by radial and non-radial pulsations in long-period variable stars (see *e.g.*, Soszyński *et al.* 2013, Iwanek *et al.* 2022).

Rotating stars are characterized by significant changes in their mean brightness compared to their rotational variability, so any measurements of their astrophysical properties should be conducted after removing the long-term trend. To address this, we applied the Savitzky-Golay filter (SG, Savitzky and Golay 1964) to remove the trend from the data. Then, we measured the rotation periods using two methods: by utilizing the FNPEAKS* code based on the standard discrete Fourier transform for unevenly spaced data (Kurtz 1985), and by employing the Fourier-like least-squares spectral analysis proposed by Lomb (1976) and Scargle (1982), which is frequently used in astronomy. A detailed discussion on the measurement of the rotation period can be found in Iwanek *et al.* (2019).

In the first step of the selection and classification procedure, we removed from the sample stars already classified and published in the OGLE Collection of Variable Stars[†] (OCVS). In total, we removed 160 objects (mainly non-spotted ellipsoidal and eclipsing variables, and several type II Cepheids). Next, we verified each light curve (unfolded and phase-folded) through visual inspection. If the rotation periods found using the above-described methods differed significantly (their ratio was outside the range of 0.95-1.05), then we phased the light curve with both periods and visually checked which one phased the light curve better. In some cases, the rotation period required manual fine-tuning. The selected and corrected periods were then considered as final.

The above-mentioned procedure enhances the accuracy of the majority of mea-

*<http://helas.astro.uni.wroc.pl/deliverables.php?active=fnpeaks>

†<https://www.astrouw.edu.pl/ogle/ogle4/OCVS/>

sured rotation periods through a meticulous verification process. The visual inspection of light curves allowed us for the identification and correction of anomalies that might eluded automated methods. By comparing periods and fine-tuning them, we ensured that the most consistent and a reliable value was determined. The rotation period was measured based on the data from the fourth phase of the OGLE project, as in this phase the light curves have the most uniform coverage. Nevertheless, we acknowledge that the actual period may differ slightly for individual objects from the one provided in our collection. Studying the rotation periods in each OGLE phase separately, and even in individual observational seasons, can provide valuable insights into changes in the rotation period and the evolution of magnetic activity.

During this verification, we removed 910 objects from the sample because they did not meet the criteria for rotating (spotted) variables. These were mainly semi-regular (pulsating) variables, ellipsoidal or eclipsing (but non-spotted) variables, artifacts from bright stars, or constant stars. We also removed candidates for chemically peculiar stars (called Ap, or more general CP), because they will be the subject of a separate study. Ultimately, we classified 18 443 stars as rotating (spotted) variables. The in-sky distribution of all discovered rotating variables is presented in Fig. 1.

4. Determination of Mean Magnitudes and Amplitudes

For the classified stars, we measured the mean magnitudes in both the *I*- and *V*-bands (if the light curve in the *V*-band was available). First, we transformed the light curve from magnitudes to flux. Then, we removed the trend using the SG filter, and we rejected outliers deviating by more than 3σ from the mean flux. After these preparation steps, we measured the mean flux and converted back the light curves and mean flux to magnitudes.

To measure the brightness amplitude in both OGLE bands (if the light curve in the *V*-band was available), we used the method described in Iwanek *et al.* (2019). We divided the light curve into bins containing at least 200 epochs (if there were more than 200 epochs, otherwise all epochs constituted one bin) and covering at least five rotation cycles, as Mathur *et al.* (2014) identified such bins as optimal for active stars. Then, we calculated the difference between the 95th and 5th percentiles of the brightness distribution in each bin. The final amplitude was determined as the median of differences calculated in all bins, divided by the distance between the above-mentioned percentiles, which is 0.9. Both parameters, *i.e.*, the mean magnitude and amplitudes were measured based on the OGLE-IV light curves, as in this phase the light curves have the most uniform coverage.

5. The OGLE Collection of Rotating Variables toward the Galactic Bulge

We present the OGLE collection of rotating (spotted) stars discovered toward the Galactic bulge, which ultimately contains 18 443 objects. This is the first cata-

Table 1

File ident.dat with equatorial coordinates and identifications for all rotating variables

ID	R.A. [h:m:s]	Decl. [deg:m:s]	OGLE-IV ID	OGLE-III ID	OGLE-II ID	Other ID
OGLE-BLG-ROT-000001	17:12:53.64	-29:41:24.2	BLG617.25.83018	BLG363.7.41109		
OGLE-BLG-ROT-000002	17:13:00.53	-29:28:55.8	BLG617.25.76720	BLG363.6.82514		
OGLE-BLG-ROT-000003	17:13:01.76	-29:52:00.3	BLG617.16.68144	BLG363.8.12132		
OGLE-BLG-ROT-000004	17:13:03.40	-29:34:19.8	BLG617.25.67272	BLG363.6.13132		
OGLE-BLG-ROT-000005	17:13:03.60	-28:13:57.7	BLG616.25.77048			
OGLE-BLG-ROT-000006	17:13:08.32	-29:46:43.2	BLG617.16.76016	BLG363.8.83264		
OGLE-BLG-ROT-000007	17:13:21.10	-29:54:06.0	BLG617.16.9711			
OGLE-BLG-ROT-000008	17:13:25.16	-29:29:53.6	BLG617.25.17094	BLG363.6.89829		
OGLE-BLG-ROT-000009	17:13:34.90	-29:34:42.6	BLG617.24.101118	BLG363.6.26424		
OGLE-BLG-ROT-000010	17:13:35.73	-28:24:47.9	BLG616.24.67136			
OGLE-BLG-ROT-000011	17:13:38.92	-29:45:09.2	BLG617.15.107872	BLG363.8.125665		
OGLE-BLG-ROT-000012	17:13:40.17	-29:18:14.4	BLG617.32.85672	BLG363.5.129784		
OGLE-BLG-ROT-000013	17:13:41.96	-30:15:53.3	BLG617.07.60080			
OGLE-BLG-ROT-000014	17:13:42.34	-29:48:57.9	BLG617.15.74001	BLG363.8.62592		
OGLE-BLG-ROT-000015	17:13:42.80	-28:00:37.6	BLG616.32.66570			
OGLE-BLG-ROT-000016	17:13:45.29	-29:34:05.5	BLG617.24.75365	BLG363.6.30704		
OGLE-BLG-ROT-000017	17:13:51.20	-28:12:23.4	BLG616.24.92498			
OGLE-BLG-ROT-000018	17:13:51.46	-29:22:46.3	BLG617.32.53344	BLG363.4.40825		
OGLE-BLG-ROT-000019	17:13:52.40	-29:43:22.3	BLG617.24.30037	BLG363.2.1704		
OGLE-BLG-ROT-000020	17:13:52.50	-29:53:54.4	BLG617.15.37841			

Table presents only the first twenty rows for guidance regarding their form and content.

log of rotating variables in the history of astronomy with such long (at least 12 yr) time-series photometry in I - and V -band. It is indisputably one of the best existing photometric datasets for studying stellar activity, including activity cycles. The data are available through the OGLE website:

- <https://www.astrouw.edu.pl/ogle/ogle4/OCVS/blg/rot/> – the whole dataset.
- <https://ogledb.astrouw.edu.pl/ogle/OCVS/> – user-friendly search engine for the entire OGLE Collection of Variable Stars.

Table 2

File `rot.dat` containing mean magnitudes and brightness amplitudes in V - and I -bands, as well as rotation periods

ID	V [mag]	A_V [mag]	I [mag]	A_I [mag]	P [d]
OGLE-BLG-ROT-000001	17.989	0.208	16.026	0.167	38.760531
OGLE-BLG-ROT-000002	20.947	0.786	19.163	0.646	3.927652
OGLE-BLG-ROT-000003	17.929	0.556	15.928	0.192	86.192261
OGLE-BLG-ROT-000004	18.054	0.187	16.341	0.126	35.143542
OGLE-BLG-ROT-000005	17.440	0.222	15.603	0.203	51.283989
OGLE-BLG-ROT-000006	19.852	0.206	18.013	0.191	4.294912
OGLE-BLG-ROT-000007	19.646	0.478	17.571	0.374	13.898817
OGLE-BLG-ROT-000008	19.565	0.308	17.978	0.211	7.720678
OGLE-BLG-ROT-000009	19.943	0.383	17.974	0.267	2.094063
OGLE-BLG-ROT-000010	21.110	1.160	18.953	0.576	4.101264
OGLE-BLG-ROT-000011	18.659	0.519	16.713	0.159	29.043105
OGLE-BLG-ROT-000012	19.571	0.349	17.609	0.299	11.729599
OGLE-BLG-ROT-000013	17.997	0.215	15.998	0.163	86.192261
OGLE-BLG-ROT-000014	19.107	0.307	17.178	0.188	41.002912
OGLE-BLG-ROT-000015	18.886	0.388	16.909	0.327	21.418297
OGLE-BLG-ROT-000016	18.485	0.253	16.709	0.162	70.625070
OGLE-BLG-ROT-000017	19.813	0.304	18.206	0.382	4.825298
OGLE-BLG-ROT-000018	19.303	0.332	17.501	0.261	10.284098
OGLE-BLG-ROT-000019	–	–	18.895	0.516	2.565629
OGLE-BLG-ROT-000020	18.498	0.142	16.626	0.159	18.791846

The sign "–" in the columns of V and A_V means, that the light curve in the V -band is not available. Table presents only the first twenty rows for guidance regarding their form and content.

The websites of the OGLE collection of rotating variables are structured as follows. The file `ident.dat` contains the list of stars with their unique identifier: OGLE-BLG-ROT-NNNNNN, where NNNNNN is a six-digit number, J2000 equatorial coordinates, identifications in the OGLE-II, OGLE-III and OGLE-IV

databases, and designations taken from external catalogs, *i.e.*, the International Variable Star Index[‡] (VSX, Watson *et al.* 2006) and ASAS-SN (Shappee *et al.* 2014, Jayasinghe *et al.* 2020). In the file `rot.dat`, we provide observational parameters for each star – the rotation period, mean magnitudes and amplitudes in the *I*- and *V*-band. The file `remarks.txt` contains comments on interesting stars (with identifiers from OCVS). The file `remarks.txt` will be updated in the future on some interesting, unusual objects. In Tables 1, 2 and 3, we present the first twenty rows from the files `ident.dat`, `rot.dat`, and `remarks.txt`, respectively, for guidance regarding their form and content.

Table 3

File `remarks.txt` containing comments on some interesting objects, with identifiers from other OGLE catalogs

ID	remark	other OGLE ID
OGLE-BLG-ROT-000965	RSCVn	OGLE-BLG-ECL-032766
OGLE-BLG-ROT-001092	RSCVn	OGLE-BLG-ECL-036149
OGLE-BLG-ROT-001820	RSCVn	OGLE-BLG-ECL-055958
OGLE-BLG-ROT-003288	RSCVn	OGLE-BLG-ECL-095740
OGLE-BLG-ROT-004213	flares	
OGLE-BLG-ROT-004667	flares	
OGLE-BLG-ROT-004832	flares	
OGLE-BLG-ROT-005253	flares	
OGLE-BLG-ROT-005282	RSCVn	
OGLE-BLG-ROT-005373	flares	
OGLE-BLG-ROT-005511	flares	
OGLE-BLG-ROT-005552	flares	
OGLE-BLG-ROT-005594	flares	
OGLE-BLG-ROT-005784	flares	
OGLE-BLG-ROT-005997	flares	
OGLE-BLG-ROT-006123	RSCVn	
OGLE-BLG-ROT-006165	flares	
OGLE-BLG-ROT-006255	flares	
OGLE-BLG-ROT-006327	flares	
OGLE-BLG-ROT-006329	RSCVn	OGLE BLG-ECL-170709

Table presents only the first twenty rows for guidance regarding their form and content.

The subdirectory `fcharts/` contains finding charts for all objects. Each finding chart is a $60' \times 60'$ subframe of the OGLE *I*-band reference image, oriented with north at the top and east at the left. The object is identified with a white cross in the center of the finding chart.

[‡]<https://www.aavso.org/vsx/index.php>

Table 4

Statistics about the number of epochs in the light curves, separately for each OGLE phase, with division into bands

Phase	Band	Med.	Max.	No. of light curves
OGLE-II	<i>I</i>	263	537	1550
OGLE-III	<i>I</i>	629	2540	13 532
OGLE-IV	<i>I</i>	2053	17 682	18 443
OGLE-II	<i>V</i>	8	18	1476
OGLE-III	<i>V</i>	5	41	13 119
OGLE-IV	<i>V</i>	144	253	17 873

In the subdirectories `phot_ogle2/`, `phot_ogle3/`, and `phot_ogle4/`, we provide all available time-series photometry in the *I*-band and *V*-band (if available) from the OGLE-II (1997-2000), OGLE-III (2001-2009), and OGLE-IV (2010-2024) phases, respectively. The data from different phases were calibrated separately to the standard Johnson-Cousins photometric system. When using the OGLE data, it is necessary to take into account that there may be a zero-point offset between the light curves from different phases. Usually, the uncertainties of the OGLE photometric calibrations do not exceed 0.05 mag. If it is necessary to merge the light curves, such an offset should be considered in the analysis.

During the preparation of the data for the catalog, we decided not to remove any outlying measurements from the light curves published in this collection. In the case of rotating stars, this is particularly challenging as flares or eclipses may occur, which can appear as outliers but may not be so. Therefore, during analyses using data from the collection, we encourage the reader to independently assess whether outlying measurements are genuine phenomena or just outliers, that could be removed.

The *I*-band light curves are available for all variables from the collection, while the *V*-band are available for 97% rotating stars (17 873 objects). Statistics regarding the light curves in both bands from the various phases of the OGLE project are presented in Table 4. In Fig. 2, we present three example light curves of rotating variables, with different coverage of the OGLE observations.

5.1. Crossmatch with Other Catalogs of Variable Stars

We crossmatched our sample of rotating variables with two external catalogs: VSX and ASAS-SN. We searched for objects around our stars' coordinates within a radius of 5'' for VSX and 1'' for ASAS-SN.

We identified 350 counterparts to our objects in the VSX. Most of these objects (342 out of 350) are classified in the VSX as ROT (rotating variables) or RS

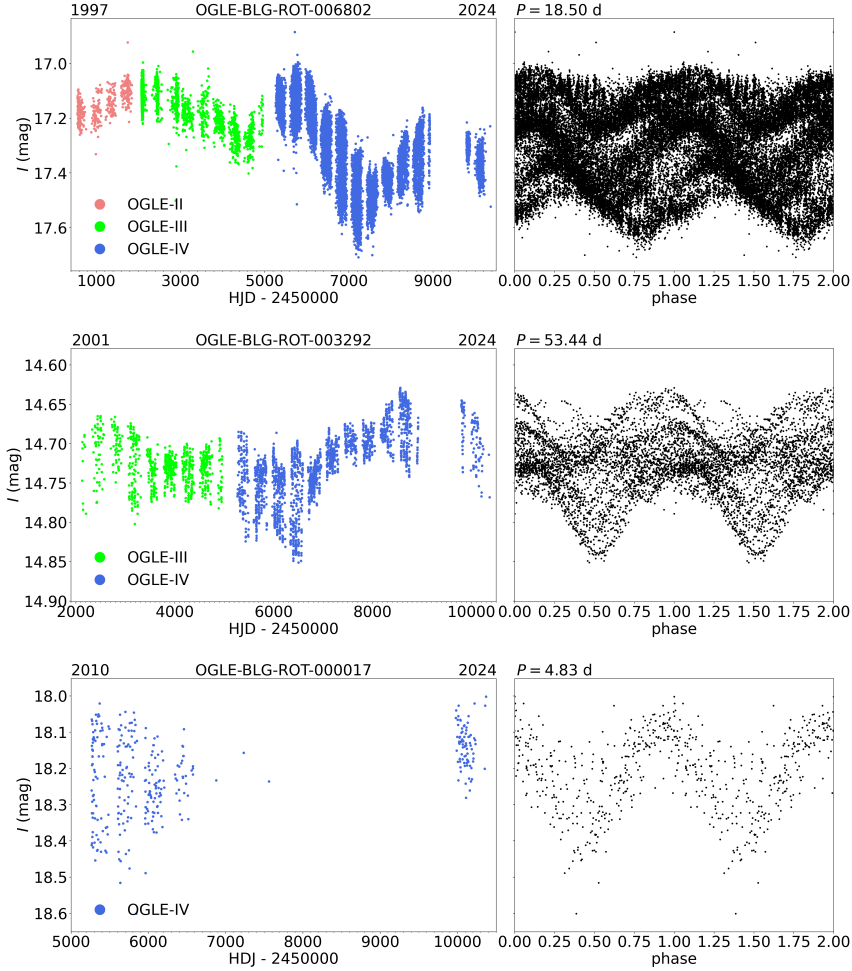


Fig. 2. Three examples of rotating variables from our collection, ordered by the number of epochs in light curves. *Top row*: a well-covered light curve of rotating variable OGLE-BLG-ROT-006802 containing 19 939 epochs that span 27 yr (from 1997 to 2024). *Middle row*: a medium-covered light curve of rotating variables OGLE-BLG-ROT-003292 containing 3173 epochs that span 23 yr (from 2001 to 2024). *Bottom row*: a poorly-covered light curve of rotating variable OGLE-BLG-ROT-000017 containing 333 epochs that span 14 yr (from 2010 to 2024). In the *left panels*, we show unfolded light curves, while in the *right panels*, we show phase-folded light curves with rotation period P indicated above the plots. The dates at the tops of the unfolded light curves mark the year when the observations started and the year of the last used observations in the collection. Different OGLE phases are marked with different colors (red, green, and blue).

(RS CVn-type variables). We checked stars with different classifications and confirmed that all of them are rotating variables. For 316 stars, the periods reported in the VSX are consistent with the periods measured in this paper to within 5%. For the remaining stars, we checked both periods and confirmed that the ones we measured were correct.

In the ASAS-SN catalog, we found 175 counterparts to objects from our collection. Most of the objects (166 out of 175) are classified by the ASAS-SN team

as ROT (rotating variables) or VAR (variable stars). We checked the remaining nine objects and confirmed that all of them are rotating variables. Only 37 stars have a period reported in the ASAS-SN catalog, and 8 of them have a period consistent with the period measured by us. We checked the remaining 29 objects and confirmed that the periods we measured were correct.

5.2. Observational Parameters of Rotating Stars

In Fig. 3, we present the distributions of rotation periods (left panel), mean brightnesses (middle panel), and amplitudes (right panel). Stars with rotation periods shorter than ≈ 2 d typically have smaller amplitudes (up to about 0.2 mag) and are mostly dwarfs. Giants begin to dominate from a rotation period longer than 2 d onwards (see *e.g.*, Fig. 11 in Iwanek *et al.* 2019). The peak of the rotation period distribution is around 50 d.

The wide range of rotation periods suggests that the level of magnetic activity is not dependent on the rotation velocity. The truncation of the distribution at a rotation period of just over 100 d is a result of the selection effect and arises from the fact that this collection of spotted variables is mostly a by-product of searches for variables of other types.

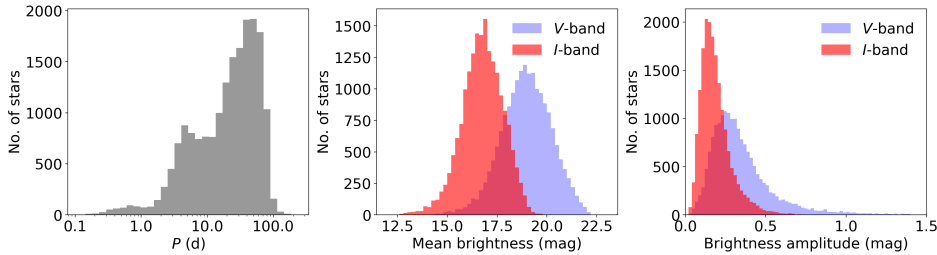


Fig. 3. Distributions of observational parameters of rotating variables. *Left panel*: distribution of rotation period. *Middle panel*: distribution of mean brightness in the *I*-band and *V*-band. *Right panel*: distribution of amplitude in the *I*-band and *V*-band.

The mean brightness range in the *I*-band is between ≈ 12.5 mag and 20 mag, while in the *V*-band the mean brightness ranging between ≈ 15 mag and 22.5 mag. The peak of mean brightness distribution in the *I*-band is around 16.9 mag, while in the *V*-band, it is at 18.9 mag.

The distribution of amplitudes is much narrower in the *I*-band than in the *V*-band. In the *I*-band, we observe amplitudes ranging from a few mmag to about 0.7 mag, with a peak at 0.13 mag. For the *V*-band, the distribution is much broader, ranging from a few mmag to over 1 mag, with a peak at 0.25 mag. In the *V*-band, active regions (mainly spots) have a greater impact on the total light reaching us from the star. The width of the amplitude distribution in the *V*-band relative to the *I*-band may be slightly distorted due to the significantly smaller number of measurements in the *V*-band, and thus less well-measured amplitudes.

5.3. Purity and Completeness of the Collection

The purity of our collection is very high due to the method of selecting rotating stars, *i.e.*, visual inspection and final confirmation of classification correctness by the human eye. As for completeness, we do not even attempt to estimate it. Recent studies show that even 8% of giants exhibit magnetic activity (Gaulme *et al.* 2020). Additionally, magnetic activity is a dynamic process with a relatively short time scale compared to other astrophysical processes, *e.g.*, pulsations. It can fade away and reappear over time, so detecting it depends on the time when we observe a given star. An example of such a phenomenon is the well-known Maunder Minimum, which occurred from 1645 to 1715, during which a significantly lower number of sunspots (by several orders of magnitude) were observed compared to a similar period in modern times (Spörer 1889, Maunder 1922, Eddy 1976, Hayakawa *et al.* 2024). The completeness of this collection can certainly be improved, and we intend to supplement the collection in the future.

5.4. Stars with over 20 years of Photometric Data

In our collection of rotating stars, 1512 objects have been continuously observed since 1997. This means that for each of these stars, time-series photometry is available from the second, third, and fourth phases of the OGLE project. For 12 020 objects we have data from OGLE-III and OGLE-IV phases, covering the time range from 2001 to 2024. For nearly one-third of the variables in the collection, the data are available only from the fourth phase of the OGLE project, which spans over 12 yr of continuous observations (from 2010 to 2024).

Almost all the light curves published in this collection are ideal datasets for measuring and studying activity cycles. Reinhold *et al.* (2017) studying stars from the Kepler satellite, detected activity cycles with lengths ranging from 0.5 yr to 6 yr. The time span of the OGLE observations and their dense coverage of the light curves make this dataset unique and may allow the detection of activity cycles even as long as the solar activity cycle, *i.e.*, 11 yr or more. In Figs. 4–10, we present 35 examples of rotating variables with the longest time-series photometry, *i.e.*, since 1997 to 2024.

In Figs. 4–10, we present 35 examples of rotating variables with the longest time-series photometry, *i.e.*, since 1997 to 2024. In the left panels, we show unfolded light curves, while in the right panels, we show phase-folded light curves with rotation period P indicated above the plots. The dates at the tops of the unfolded light curves mark the year when the observations started and the year of the last used observations in the collection. Different OGLE phases are marked with different colors (red, green, and blue).

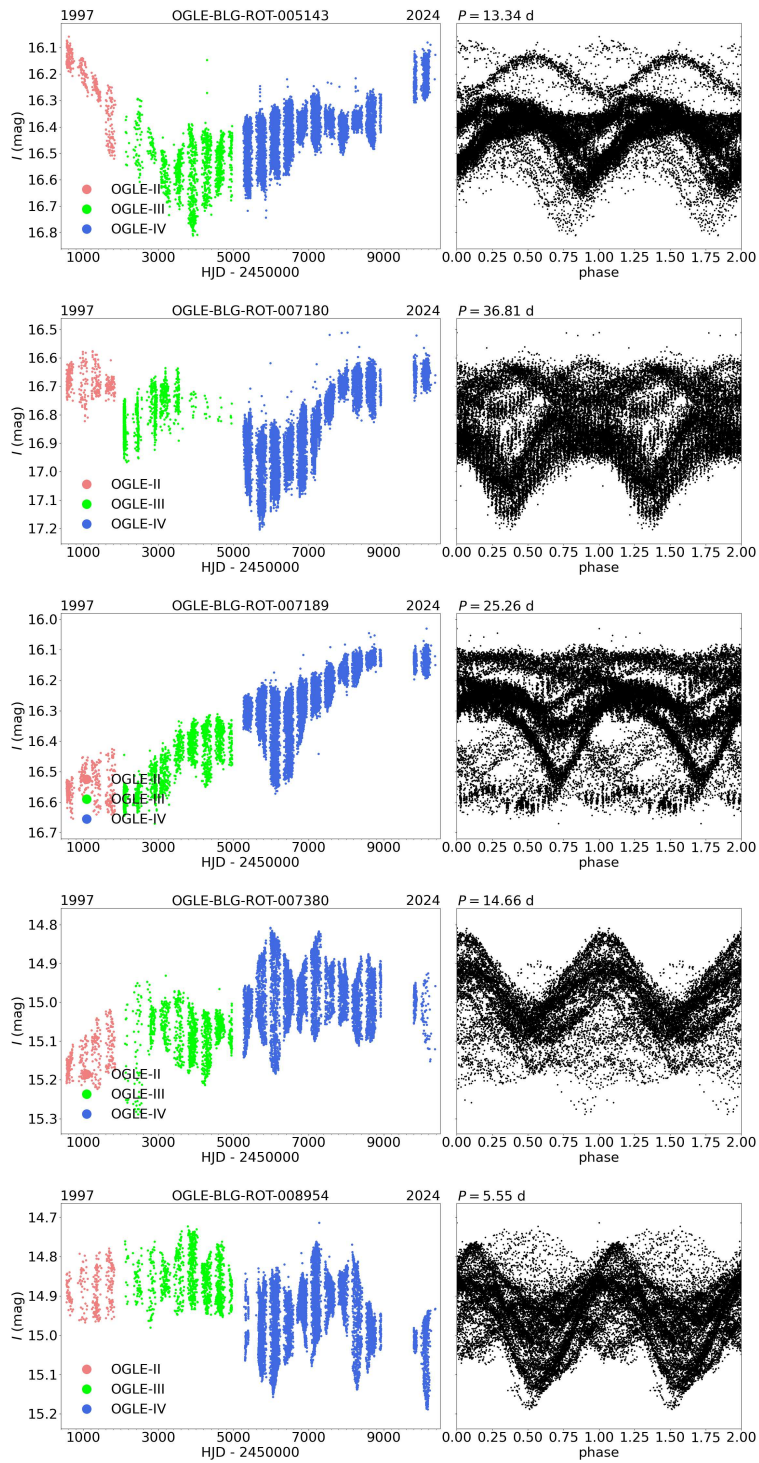


Fig. 4. Five examples of rotating variables from our collection, with the longest time-series photometry, spanning from 1997 to 2024.

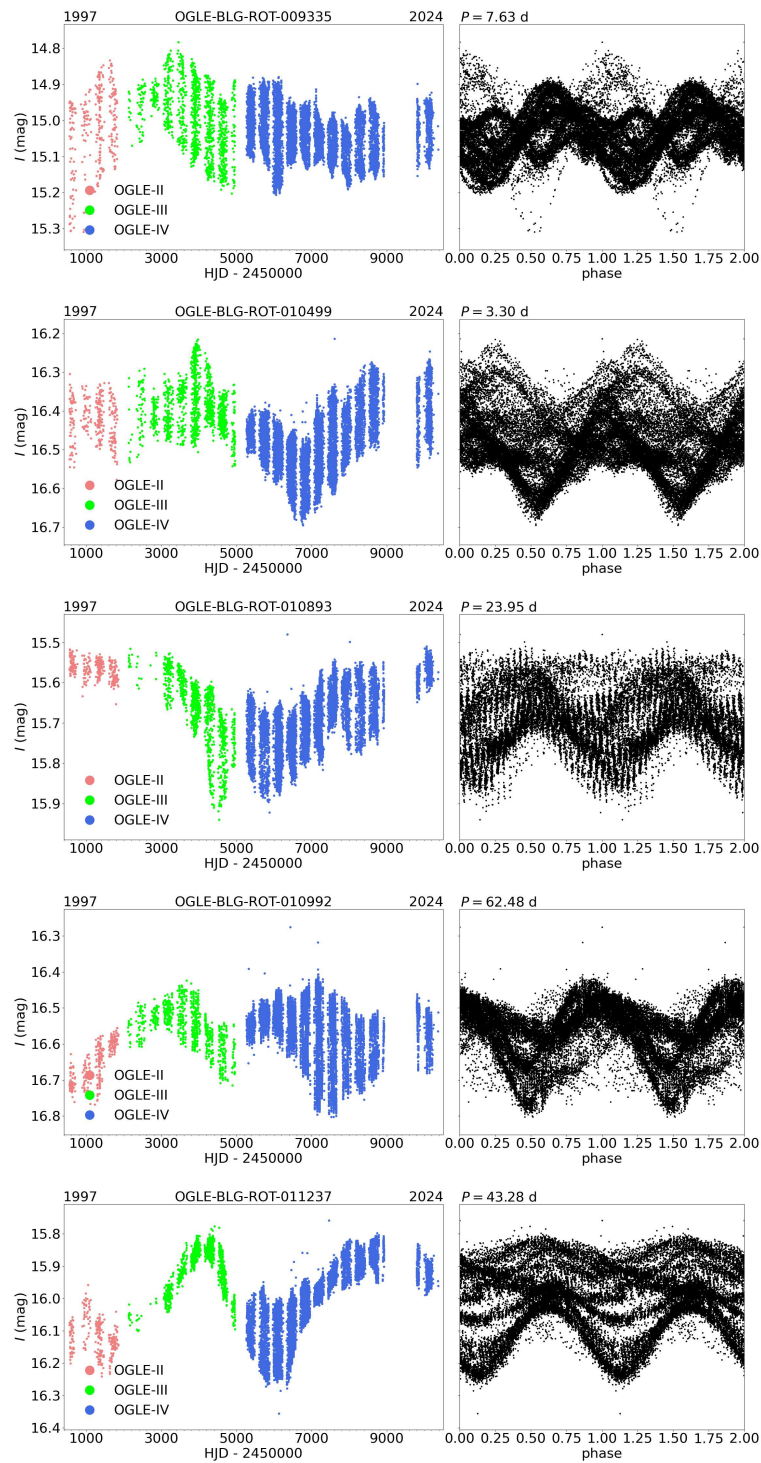


Fig. 5. Same as Fig. 4, but five other examples of rotating variables are presented.

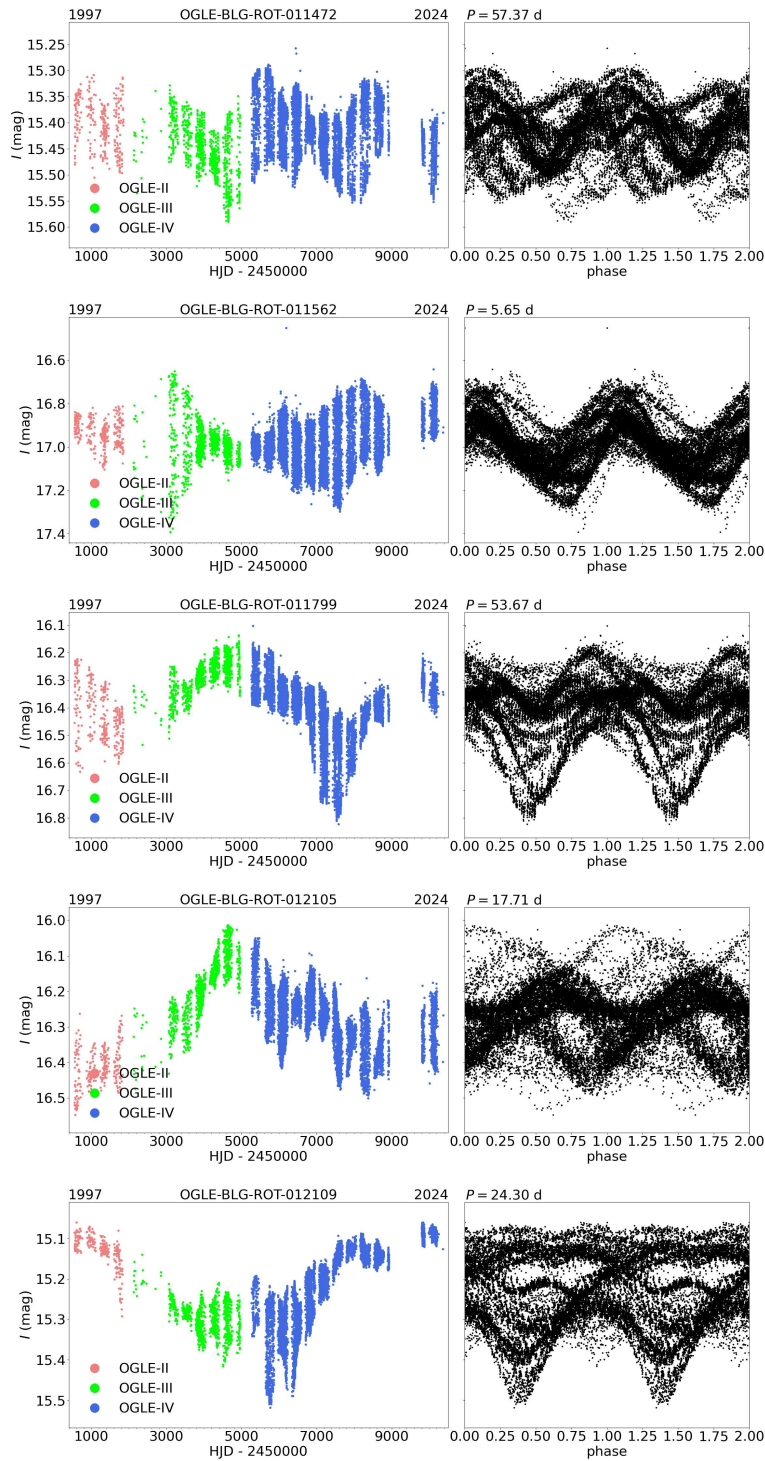


Fig. 6. Same as Fig. 4, but five other examples of rotating variables are presented.

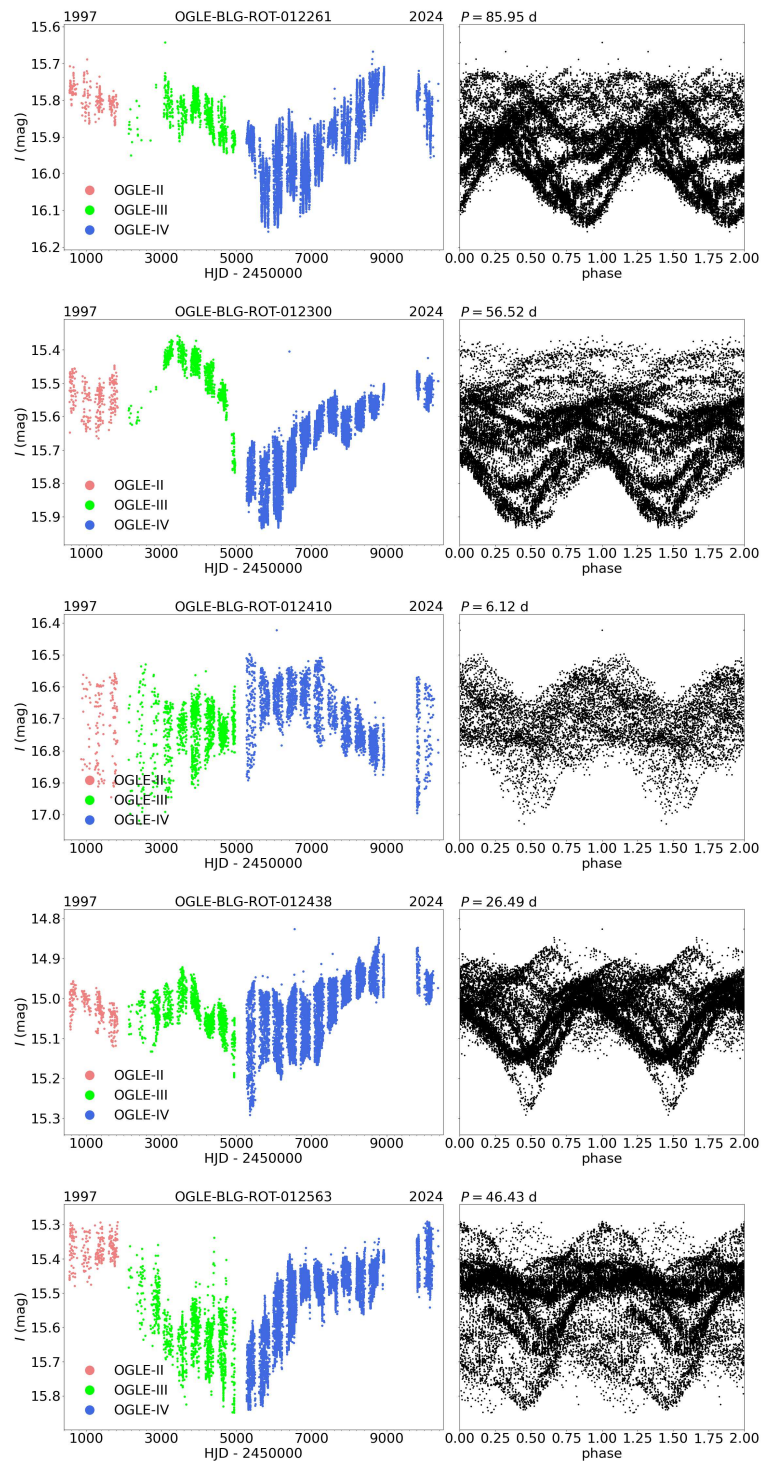


Fig. 7. Same as Fig. 4, but five other examples of rotating variables are presented.

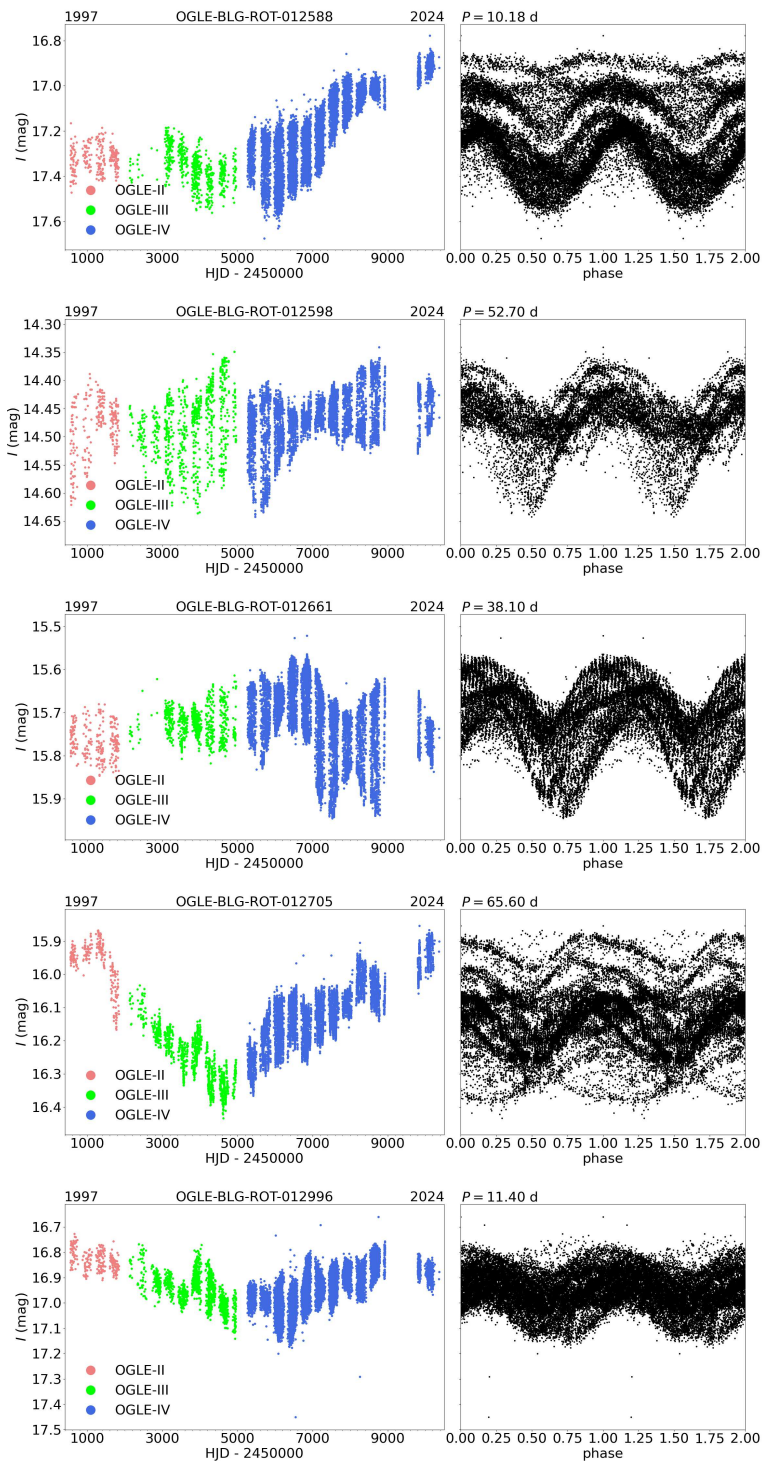


Fig. 8. Same as Fig. 4, but five other examples of rotating variables are presented.

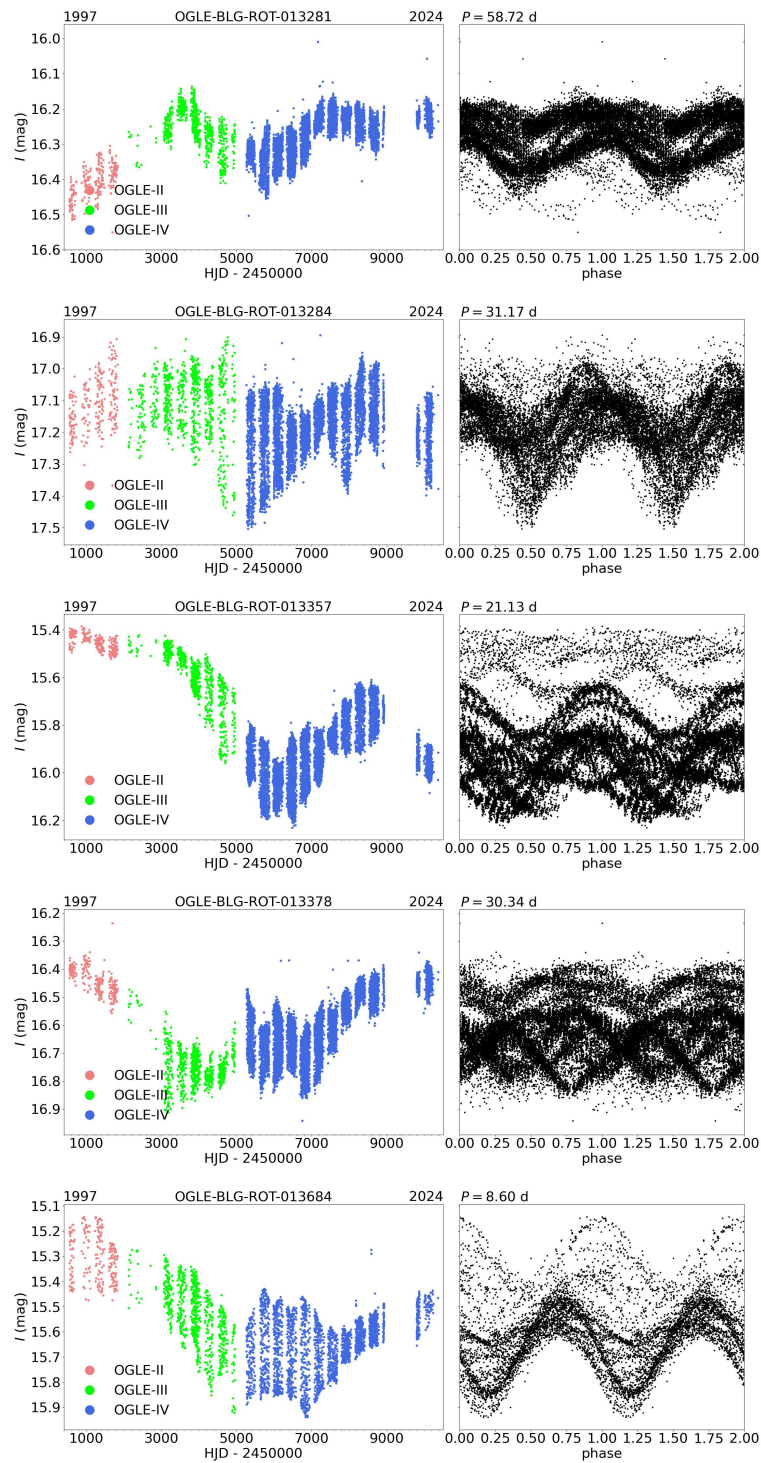


Fig. 9. Same as Fig. 4, but five other examples of rotating variables are presented.

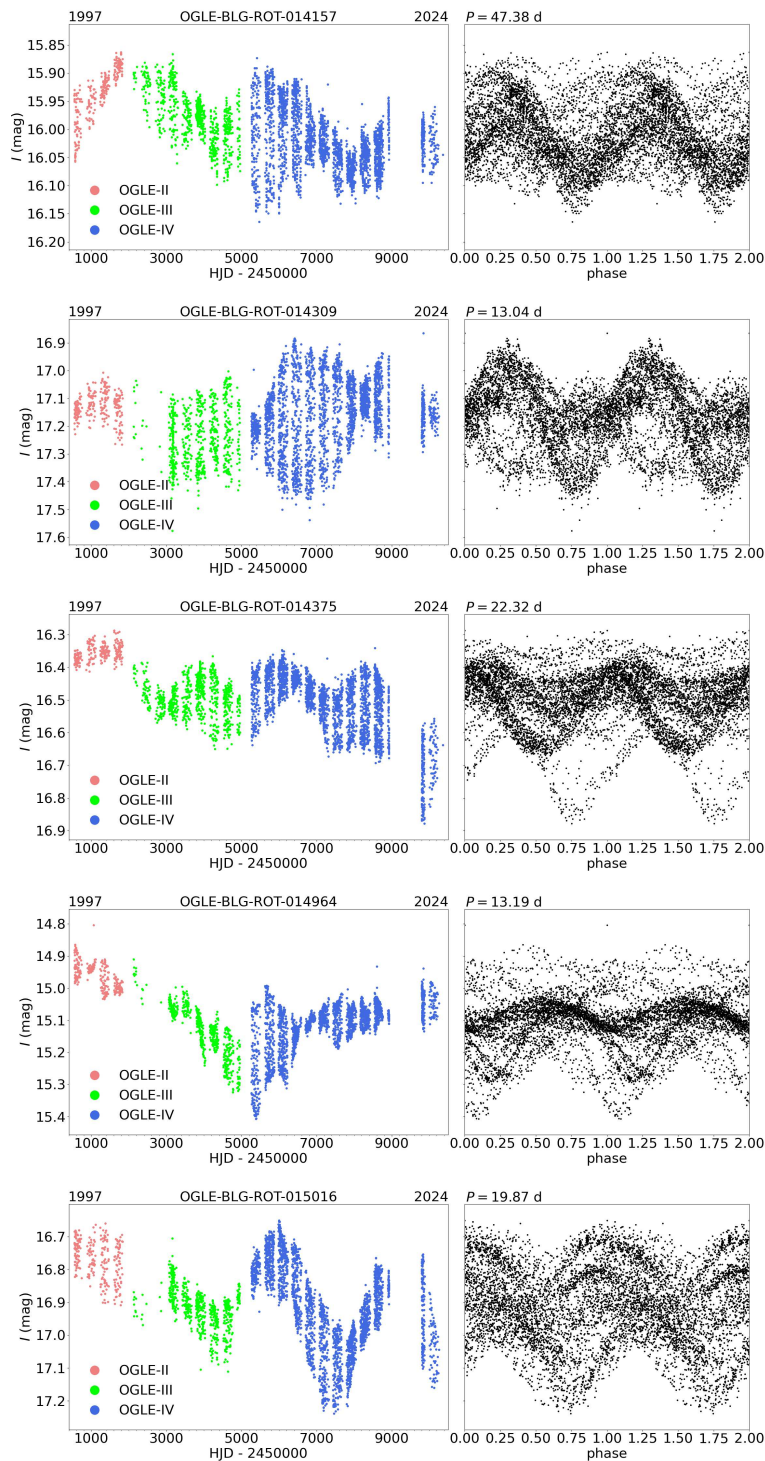


Fig. 10. Same as Fig. 4, but five other examples of rotating variables are presented.

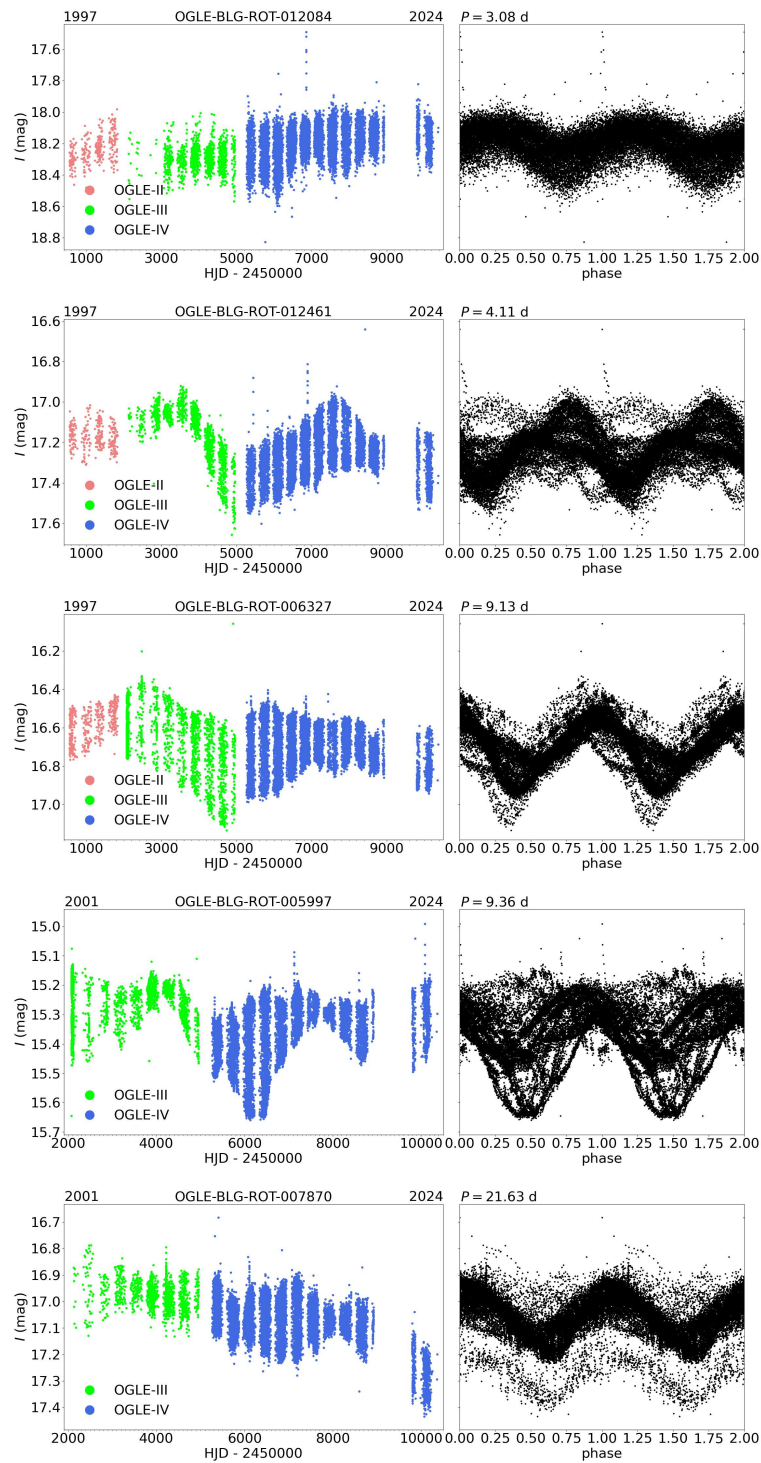


Fig. 11. Five examples of stars in which variability we detected flares activity.

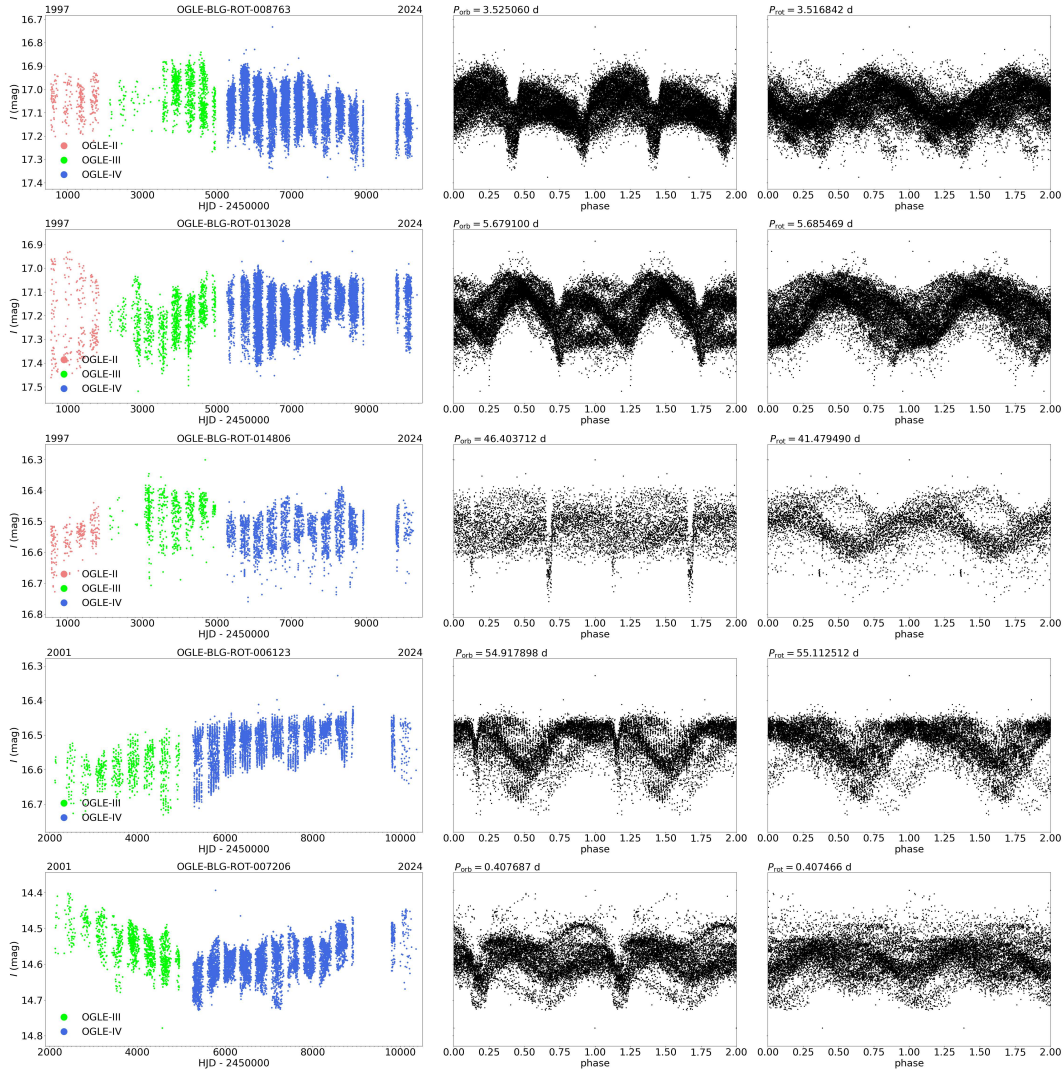


Fig. 12. Five examples of RS CVn binaries from our collection.

5.5. Flaring Stars and Eclipsing Binaries with Spots

Flares are another indicator of stellar magnetic activity, following stellar spots. Classical flares on cool stars are phenomena of the sudden release of the energy stored by the magnetic field in active regions of stars through magnetic reconnection. Recent studies show that flares also occur on hot stars (Balona 2012, Bai and Esamdin 2020), but the mechanism producing flares is slightly different compared to cool stars and is related to shocks and radiatively driven winds. In general, flare activity depends on the strength of the magnetic field, which can be stronger with higher rotational velocity. Flares are usually observed as asymmetric brightenings in the light curves (rapid rise and slow decline). However, releases of energy ob-

served as flares can also be observed as symmetric rise and decline (Mróz 2023). An analysis of the statistical properties of flares discovered in the OGLE data can be found in Iwanek *et al.* (2019). In Fig. 11, we present five objects from our collection in which we detected flare activity.

RS CVn-type stars are binaries consisting of a hot primary component, which is a subgiant or giant of spectral type F-K, and a cooler secondary component, usually a dwarf or a subgiant of type G-M (Biermann and Hall 1976). RS Canum Venaticorum is the prototype of the whole class, and its light variations were first observed by Hoffmeister (1915). The nature of the RS CVn objects are very complex and is caused by eclipses (in case of the high inclination), ellipticity, but also spots. In the system, at least one component (usually the primary one) is heavily spotted (with spots covering even 10% of the stars' surface, Vogt *et al.* 1999). RS CVn stars also show flare activity (Pietrukowicz *et al.* 2013, Kunt and Dal 2017, Lahiri *et al.* 2023), and activity cycles (Martínez *et al.* 2022). The stars in the system are usually tidally synchronized, meaning that the active primary component rotates in exact synchronization with the orbital motion (*i.e.*, the orbital period is equal to the average rotation period of the primary component). However, due to differential rotation and the evolution of starspots on the stellar surface, the period of the observed starspot wave can be slightly different from the orbital period. Yet, it is estimated that about 15% of RS CVn stars do not rotate synchronously or even nearly synchronously (Hall and Henry 1990), and the ratio of the rotation period ($P = P_{\text{rot}}$) to the orbital period (P_{orb}) can reach even a factor of several. Examples include two extreme systems: λ And with the ratio equal to 2.6 and V4138 Sgr with the ratio equal to 4.6 (Hall 1992).

In Fig. 12, we present five examples of RS CVn-type stars from our collection. In this figure, we show phase-folded light curves with orbital and rotation periods. In the left panel, we show unfolded light curves, while in the middle and right panels, we show phase-folded light curves with orbital period P_{orb} and rotation period P_{rot} , respectively. The periods are indicated above the phase-folded plots. The dates at the tops of the unfolded light curves mark the year when the observations started and the year of the last used observations in the collection. Different OGLE phases are marked with different colors (red, green, and blue).

6. Conclusions

We presented the collection of over 18 000 rotating variables with clear magnetic field manifestation, *i.e.*, spots or flares. With this paper, we provide long-term, time-series photometry in the Cousins *I*- and Johnson *V*-band obtained from the second phase to the current fourth phase of the OGLE project (since 1997), finding charts, and basic observational parameters, *i.e.*, equatorial coordinates, rotation periods, mean brightness and amplitudes in both bands. The meticulous classification process, involving semi-automatic methods and visual inspection, ensures the high

purity of the collection. This collection provides an invaluable dataset laying the groundwork for future studies of magnetic activity, including activity cycles.

Acknowledgements. This work has been supported by the Polish National Science Centre grant PRELUDIUM 18 No. 2019/35/N/ST9/02474 to P.I. I.S. has been supported by the National Science Center, Poland, grant No. 2022/45/B/ST9/00243. For the purpose of Open Access, the author has applied a CC-BY public copyright license to any Author Accepted Manuscript (AAM) version arising from this submission. This research has made use of the International Variable Star Index (VSX) database, operated at AAVSO, Cambridge, Massachusetts, USA. We would like to thank OGLE observers for their contribution to the collection of the photometric data used in this paper.

REFERENCES

- Aerts, C., Mathis, S., and Rogers, T.M. 2019, *Ann. Rev. Astron. Astrophys.*, **57**, 35.
- Bai, J.-Y., and Esamdin, A. 2020, *ApJ*, **905**, 110.
- Baliunas, S.L., Hartmann, L., Noyes, R.W., *et al.* 1983, *ApJ*, **275**, 752.
- Balona, L.A. 2012, *MNRAS*, **423**, 3420.
- Barnes, S.A. 2007, *ApJ*, **669**, 1167.
- Biermann, P., and Hall, D.S. 1976, *Structure and Evolution of Close Binary Systems*, **73**, 381.
- Charbonneau, P. 2013, “Saas-Fee Advanced Course” p.39.
- Chowdhury, S., Joshi, S., Engelbrecht, C.A., *et al.* 2018, *Astrophys. and Space Sci.*, **363**, 260.
- Crowley, J., Wheatland, M.S., and Yang, K. 2024, *MNRAS*, **530**, 457.
- Davenport, J.R.A. 2016, *ApJ*, **829**, 23.
- Davenport, J.R.A., Covey, K.R., Clarke, R.W., *et al.* 2019, *ApJ*, **871**, 241.
- Distefano, E., Lanzafame, A.C., Brugaletta, E., *et al.* 2023, *A&A*, **674**, A20.
- Drake, A.J. 2006, *AJ*, **131**, 1044.
- Eddy, J.A. 1976, *Science*, **192**, 1189.
- Gaulme, P., Jackiewicz, J., Spada, F., *et al.* 2020, *A&A*, **639**, A63.
- Gilliland, R.L., and Fisher, R. 1985, *PASP*, **97**, 285.
- Hall, D.S. 1992, *ASP Conf.*, **103**, 27.
- Hall, D.S., and Henry, G.W. 1990, in: “Active Close Binaries Proceedings”, NATO Advanced Study Institute, **319**, 287.
- Hayakawa, H., Carrasco, V.M.S., Aparicio, A.J.P., *et al.* 2024, *MNRAS*, **528**, 6280.
- Hoffmeister, C. 1915, *Astron. Nachr.*, **200**, 177.
- Irwin, J., Aigrain, S., Bouvier, J., *et al.* 2009, *MNRAS*, **392**, 1456.
- Iwanek, P., Soszyński, I., Skowron, J., *et al.* 2019, *ApJ*, **879**, 114.
- Iwanek, P., Soszyński, I., Kozłowski, S., *et al.* 2022, *ApJS*, **260**, 46.
- Jayasinghe, T., Stanek, K.Z., Kochanek, C.S., *et al.* 2020, *MNRAS*, **491**, 13.
- Kiraga, M. 2012, *Acta Astron.*, **62**, 67.
- Kiraga, M., and Stępień, K. 2013, *Acta Astron.*, **63**, 53.
- Kunt, M., and Dal, H.A. 2017, *Acta Astron.*, **67**, 345.
- Kurtz, D.W. 1985, *MNRAS*, **213**, 773.
- Lahiri, D., Rani, G.M., and Sriram, K. 2023, *Astrophys. and Space Sci.*, **368**, 90.
- Lanzafame, A.C., Distefano, E., Messina, S., *et al.* 2018, *A&A*, **616**, A16.
- Lanzafame, A.C., Brugaletta, E., Frémat, Y., *et al.* 2023, *A&A*, **674**, A30.
- Lomb, N.R. 1976, *Astrophys. and Space Sci.*, **39**, 447.
- Maeder, A., and Meynet, G. 2000, *Ann. Rev. Astron. Astrophys.*, **38**, 143.

- Martínez, C.I., Mauas, P.J.D., and Buccino, A.P. 2022, *MNRAS*, **512**, 4835.
- Mathur, S., Garcia, R.A., Ballot, J., *et al.* 2014, *A&A*, **562**, A124.
- Maunder E. W., 1922, *Journal of the British Astronomical Association*, **32**, 140.
- McQuillan, A., Mazeh, T., and Aigrain, S. 2014, *ApJS*, **211**, 24.
- Montet, B.T., Tovar, G., and Foreman-Mackey, D. 2017, *ApJ*, **851**, 116.
- Mróz, P. 2023, *Acta Astron.*, **73**, 259.
- Oláh, K., Strassmeier, K.G., Granzer, T., *et al.* 2007, *Astron. Nachr.*, **328**, 1072.
- Oláh, K., Kolláth, Z., Granzer, T., *et al.* 2009, *A&A*, **501**, 703.
- Oláh, K., Kóvári, Z., Petrovay, K., *et al.* 2016, *A&A*, **590**, A133.
- Parker, E.N. 1955, *ApJ*, **122**, 293.
- Pietrukowicz, P., Mróz, P., Soszyński, I., *et al.* 2013, *Acta Astron.*, **63**, 115.
- Reinhold, T., Reiners, A., and Basri, G. 2013, *A&A*, **560**, A4.
- Reinhold, T., and Gizon, L. 2015, *A&A*, **583**, A65.
- Reinhold, T., Cameron, R.H., and Gizon, L. 2017, *A&A*, **603**, A52.
- Reinhold, T., Shapiro, A.I., Solanki, S.K., *et al.* 2023, *A&A*, **678**, A24.
- Rivinius, T., Carciofi, A.C., and Martayan, C. 2013, *Astron. and Astrophys. Rev.*, **21**, 69.
- Roettenbacher, R.M., Monnier, J.D., Korhonen, H., *et al.* 2016, *Nature*, **533**, 217.
- Salabert, D., Garcia, R.A., Beck, P.G., *et al.* 2016, *A&A*, **596**, A31.
- Savitzky, A., and Golay, M.J.E. 1964, *Analytical Chemistry*, **36**, 1627.
- Scargle, J.D. 1982, *ApJ*, **263**, 835.
- Schwabe, H. 1844, *Astron. Nachr.*, **21**, 233.
- Schwabe, M. 1845, *Astron. Nachr.*, **22**, 365.
- Shappee, B.J., Prieto, J.L., Grupe, D., *et al.* 2014, *ApJ*, **788**, 48.
- Skumanich, A. 1972, *ApJ*, **171**, 565.
- Soszyński, I., Udalski, A., Szymański, M.K., *et al.* 2013, *Acta Astron.*, **63**, 21.
- Soszyński, I., Pawlak, M., Pietrukowicz, P., *et al.* 2016, *Acta Astron.*, **66**, 405.
- Spörer G. 1889, *Nova Acta der Ksl. Leop.-Carol. Deutschen Akademie der Naturforscher*, **53**, 281.
- Udalski, A. 2003, *Acta Astron.*, **53**, 291.
- Udalski, A., Szymański, M., Kałużny, J., *et al.* 1992, *Acta Astron.*, **42**, 253.
- Udalski, A., Kubiak, M., and Szymański, M. 1997, *Acta Astron.*, **47**, 319.
- Udalski, A., Szymański, M.K., and Szymański, G. 2015, *Acta Astron.*, **65**, 1.
- Udalski, A., Soszyński, I., Pietrukowicz, P., *et al.* 2018, *Acta Astron.*, **68**, 315.
- Vogt, S.S., Hatzes, A.P., Misch, A.A., *et al.* 1999, *ApJS*, **121**, 547.
- Watson, C.L., Henden, A.A., and Price, A. 2006, *Society for Astronomical Sciences Annual Symposium*, **25**, 47.
- Wrona, M., Ratajczak, M., Kołaczek-Szymański, P.A., *et al.* 2022, *ApJS*, **259**, 16.